European Journal of Cell Biology 96 (2017) 673–684

Contents lists available at ScienceDirect

European Journal of Cell Biology

journal homepage: www.elsevier.com/locate/ejcb

Short communication

Cellular distribution of invadopodia is regulated by nanometer scale surface protein patterns

Gizem Bati-Ayaz[a], Ali Can[a], Devrim Pesen-Okvur[b,*]

[a] Izmir Institute of Technology, Graduate Program in Biotechnology and Bioengineering, Turkey
[b] Izmir Institute of Technology, Department of Molecular Biology and Genetics, Turkey

ARTICLE INFO

Keywords:
Nanopattern
Electron beam lithography
Invadopodia
Cortactin
Golgi complex

ABSTRACT

Invadopodia are proteolytic structures formed by cancer cells. It is not known whether their cellular distribution can be regulated by the organization of the extracellular matrix or the organization of the golgi complex or whether they have an adhesion requirement. Here, we used electron beam lithography to fabricate fibronectin (FN) nanodots with isotropic and gradient micrometer scale spacings on K-casein and laminin backgrounds. Investigating cancer cells cultured on protein nanopatterns, we showed that (i) presence of FN nanodots on a K-casein background decreased percent of cells with neutral invadopodia polarization compared to FN control surfaces; (ii) presence of a gradient of FN nanodots on a K-casein background increased percent of cells with negative invadopodia polarization compared to FN control surfaces; (iii) polarization of the golgi complex was similar to that of invadopodia in agreement with a spatial link; (iv) local adhesion did not necessarily appear to be a prerequisite for invadopodia formation.

1. Introduction

The leading cause of death for cancer patients is metastasis. One of the early steps in metastasis is that tumor cells invade the surrounding matrix using their proteolytic feet, namely invadopodia. Invadopodia are actin rich cellular structures formed by invasive cancer cells (Bati and Okvur, 2014; Bowden et al., 2006; Buccione et al., 2009; Linder, 2009; Linder and Aepfelbacher, 2003). Growth factor receptor tyrosine kinase and integrin initiated signaling pathways are known to activate cortactin and induce invadopodia (Beaty et al., 2013; Destaing et al., 2011; MacGrath and Koleske, 2012; Mader et al., 2011; Oser et al., 2010; Stylli et al., 2008; Yamaguchi et al., 2005). Invadopodia can appear as structures of a few hundred nanometers and extend up to eight micrometers if the underlying matrix is thick enough (Baldassarre et al., 2003). Invadopodia also form on stiff substrates such as glass where they can be identified by molecular markers such as actin, cortactin and/or MT1-MMP (Artym et al., 2006; DesMarais et al., 2009; Oser et al., 2009; Stylli et al., 2008). Invadopodia appear to be in close proximity to the golgi complex suggesting a link between proteolytic activity and membrane transport (Baldassarre et al., 2003; Buccione et al., 2009; Caldieri and Buccione, 2010). In addition, position and orientation of golgi is modulated by micrometer scale surface patterns (Thery et al., 2006). However, it is not known whether the organization of the extracellular matrix can regulate cellular distribution of invadopodia or whether polarization of the golgi complex and invadopodia correlate. Furthermore, it is still unclear if invadopodia have an adhesive function as they lack vinculin (Gimona et al., 2008; Linder, 2009; Linder et al., 2011); it is not known whether invadopodia require local adhesion at the sites of formation.

Surface patterning techniques are diverse and their applications in cell biology have mainly focused on cell adhesion and motility (Agheli et al., 2006; Bat et al., 2015; Cavalcanti-Adam et al., 2007; Horzum et al., 2014; Pesen and Haviland, 2009). Micropatterned surfaces have been used to investigate dynamics of mechanical properties of invadopodia/podosomes (Anderegg et al., 2011; Labernadie et al., 2010; van den Dries et al., 2012). However, nano- and micro-patterned substrates are barely exploited to reveal important insights into cell biology and in particular cancer cell biology.

Here, we used electron beam lithography to fabricate surface immobilized protein nanopatterns that can mimic the *in vivo* organization of the extracellular matrix. We fabricated nanometer scale protein patterns of homogenous and gradient micrometer scale spacings. We used the patterned surfaces to determine whether the cellular distribution of invadopodia can be regulated by the organization of the

Abbreviations: FN, fibronectin; Lam, laminin; KcasFN, FN nanopatterns on a K casein background; LamFN, FN nanopatterns on a laminin background; KcasFNg, gradient FN nanopatterns on a K-casein background; LamFNg, gradient FN nanopatterns on a laminin background

* Corresponding author.
E-mail address: devrimpesen@iyte.edu.tr (D. Pesen-Okvur).

http://dx.doi.org/10.1016/j.ejcb.2017.08.001
Received 17 July 2016; Received in revised form 26 June 2017; Accepted 14 August 2017

extracellular matrix or the organization of the golgi complex or whether they have an adhesion requirement. Our results showed that both composition and organization of surface protein nanopatterns regulated invadopodia formation and distribution; polarization of invadopodia was similar to that of the golgi complex, and local adhesion did not necessarily appear to be a prerequisite for invadopodia formation.

2. Materials and methods

Unless otherwise noted, materials were obtained from Sigma, Germany.

2.1. Fabrication of protein nanopatterns

K-casein coating of silicon wafers (University Wafer, MA, USA) was performed as previously described (Pesen et al., 2007; Pesen and Haviland, 2009) with the following modifications: Silicon chips were coated with APTES (3-aminopropylethoxysilane) followed by glutaraldehyde coating and incubated with 2 mg/ml K-casein for 24 h or 0.025 mg/ml laminin for 1 h. Both unlabelled and DyLight350 or 650 (Thermofisher Scientific, Waltham, MA, USA) conjugated K-casein were used. Surfaces were patterned by electron beam lithography (eLine, Raith GmbH, Dortmund, Germany) at an accelerating voltage of 5 kV and an aperture of 30 μm. The line exposure mode was used with step size of 5 micrometer instead of the dot exposure mode to reduce exposure times. Uniform (5 micrometer spaced dots) and gradient (1–10 micrometers spaced dots) patterns were designed using the Raith software in GDSII format. After exposure, surfaces were backfilled with 0.05 mg/ ml unlabeled or DyLight350 or 650 (Thermofisher Scientific, Waltham, MA, USA) conjugated fibronectin for 1 h. Control samples contained only one type of protein: K-casein, fibronectin or laminin and were not exposed to an electron beam

2.2. Cell culture

Unless otherwise noted, cell culture materials were obtained from Biological Industries, Israel. MDA-MB-231 cells were cultured in DMEM supplemented with 10% fetal bovine serum. Cells were passaged every 2-3 days. For culture on nanopatterns, cells were first starved in Leibovitz's medium supplemented with 0.35% bovine serum albumin (GIBCO/Invitrogen, Karlsruhe, Germany) for 2 h. Then, cells were lifted with cell dissociation buffer and cultured on nanopatterns in Leibovitz's medium supplemented with 5 nM EGF for 24 h at 37 °C and 5% CO2. Cells were starved and stimulated with EGF to induce invadopodia formation. The experimental culture medium did not contain serum which contains fibronectin and other extracellular matrix proteins, and therefore can overwrite the surface protein nanopatterns.

2.3. Immunofluorescence

Cells were first fixed with 4% paraformaldehyde in phosphate buffered saline (PBS) and then permeabilized with 0.1% Triton X-100 in PBS. After blocking with 1% bovine serum albumin in PBS, cells were stained with cortactin (4F11, Millipore or H222 Cell Signaling), fibronectin (F3648 and F0791, Sigma, Germany), laminin (L9393, Sigma, Germany), golgi (A21270, Invitrogen), vinculin (V9131, Sigma, Germany) specific primary antibodies. Then cells were stained with the Alexa350, Alexa488, Alexa555 or Alexa647 fluorophore conjugated secondary antibodies and phalloidin (Molecular Probes, Eugene, OR, USA). The cells were imaged by an Olympus epifluorescence microscope with a 100X oil immersion objective or a Zeiss epifluorescence microscope with a 63X oil immersion objective.

2.4. Image analysis

Image analysis was performed by ImageJ program. Invadopodia analysis was performed using a previously described approach 39. Detection of invadopodia from immunofluorescence images was performed in a semi-automatic way. An ImageJ macro was used to threshold and detect cortactin rich spots in the immunofluorescence images for cortactin. The ROIs (region of interests) for these spots were overlaid onto the immunofluorescence images of actin and double positive spots were counted as invadopodia. In addition, all invadopodia were detected by eye in the immunofluorescence images for cortactin. The manual and macro counts of invadopodia were compared. The macro originally developed for the detection of focal adhesions identified almost all of the invadopodia per cell ($R^2 = 0.9445$, Fig. S1), there was no false positive invadopodium out of 955 cortactin spots detected by the macro in 217 cells analyzed. Yet manual inspection was used to include false negatives. The total number of invadopodia detected manually was 1065 for 217 cells. Only single cells were analyzed to exclude input from cell–cell interactions.

For polarization analysis, the partitioning of cells into two parts was performed using an ImageJ macro to draw a separation line in combination with the functions of the ROI manager tool of ImageJ (Fig. S2, Appendix). The cell was divided into two parts through a line passing through its geometric center. For gradient surfaces, the separation line aligned perpendicular to the gradient pattern. For isotropic patterned surfaces, it was parallel to any line of the nanodots. For control surfaces, there was no specific alignment of the separation line. The two parts of the cell were randomly marked as "up" and "down" except that for gradient surfaces, where "up" was for the part on the higher density of fibronectin nanodots and "down" was for the part on the lower density of fibronectin nanodots. Polarization was calculated as

$$P = 5 * [(Value\_up - Value\_down)/(Value\_up + Value\_down)].$$

The "value" was either cell area, sum of the distances of invadopodia to the cell center or the mean fluorescence intensity of the golgi complex.

Cells with polarization values between (−5 and −3.3), (−3.3 and 3.3) and (3.3 and 5) were also classified into negative, neutral and positive polarization groups, respectively.

We used sum of the distances to cell center instead of mean intensity for invadopodia because cortactin staining shows not only invadopodia but also vesicles containing cortactin in the cytosol and the cortactin at the cell membrane.

2.5. Statistical analysis

Data were processed by Excel. The number of cells per condition

Table 1
Cell area, invadopodia number per cell and invadopodia density.

	FN	Lam	KcasFN	LamFN	KcasFNg	LamFNg
Cell area (μm^2)	1234 ± 63	851 ± 56	1051 ± 74	649 ± 113	896 ± 42	561 ± 43
Inv. number per cell	4.8 ± 0.45	6.97 ± 1.16	3.62 ± 0.43	7.23 ± 1.39	4.54 ± 0.71	4.5 ± 0.68
Inv. density ($1/\mu m^2$)	0.0042 ± 0.0004	0.0076 ± 0.0012	0.004 ± 0.0005	0.0123 ± 0.0019	0.0047 ± 0.0006	0.008 ± 0.0009
n	56	31	47	13	54	16

Mean ± s.e.m values are reported. Please refer to Fig. S3 for the graphical presentation and statistically significant differences.

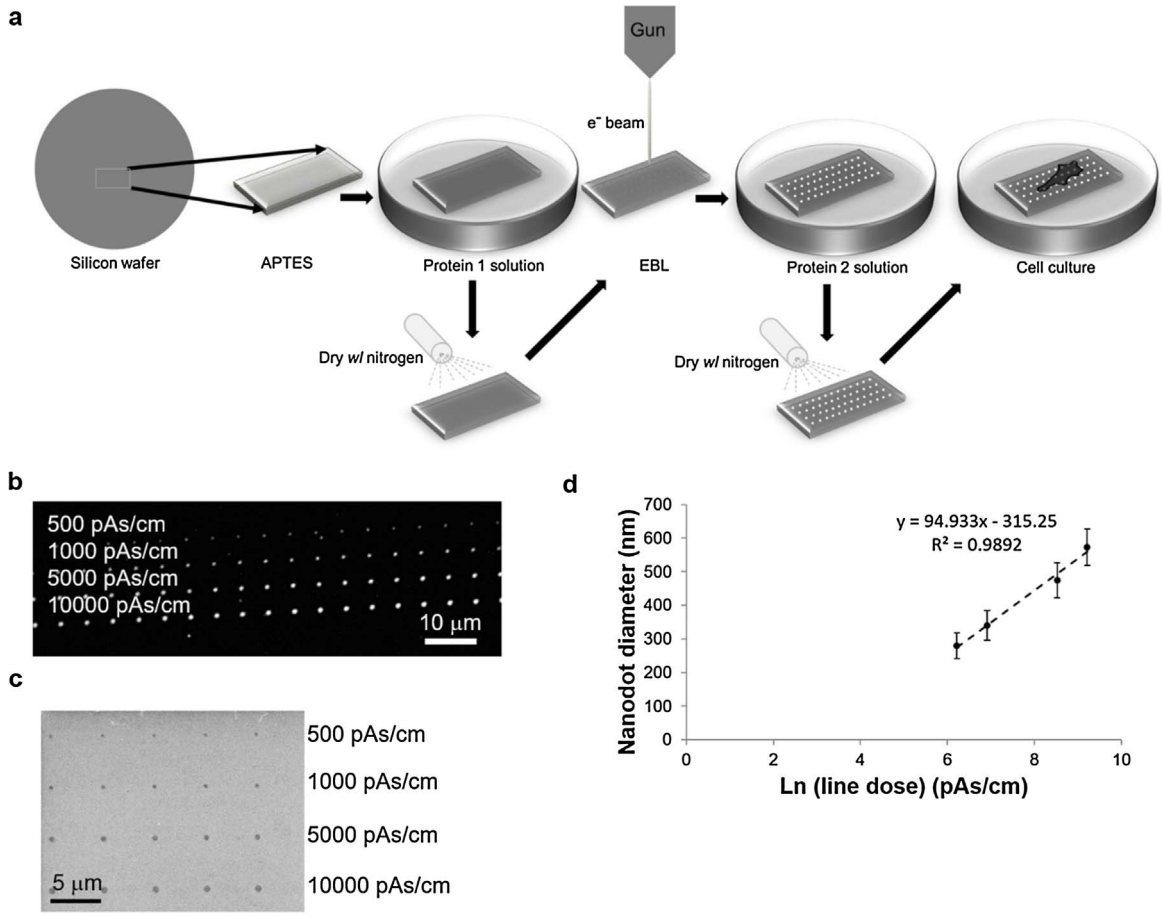

Fig. 1. Nanometer scale protein patterns fabricated using electron beam lithography. (a) Silicon wafers functionalized with APTES were coated with a protein of interest, exposed to a focused electron beam and backfilled with a second protein of interest. Finally, breast cancer cells were cultured on patterned surfaces. (b) Immunofluorescence image of fibronectin nanodots on a K-casein background. (c) Scanning electron micrograph of part of the pattern in (b). (d) Nanodot diameter depends on applied dose. Mean ± std. dev. Values are plotted.

was in the range of n = 13–69 (Tables 1 and S2). Two-tailed Mann-Whitney test (MatLab) and two sample *t*-test between percents (Stat-Calculator) was used for statistical analysis and results were presented as mean ± s.e.m. unless otherwise noted. All data is provided as an Excel file (SuppData).

3. Results and discussion

Nanometer scale protein patterns with micrometer scale spacings were fabricated using electron beam lithography (Fig. 1a) (Horzum et al., 2014; Pesen et al., 2007). Briefly, protein coated silicon surfaces were exposed to a focused electron beam and the exposed parts were then backfilled with a second protein of interest. Representative fluorescence and scanning electron microscopy images of patterned surfaces are shown in Fig. 1b and 1c. Here, line exposure mode with a step size of 5 µm rather than the dot exposure mode was used to reduce exposure times. As the applied electron beam dose increased, the diameter of the resulting protein nanodots increased, as expected (Fig. 1d, Table S1). We previously showed that cells did not adhere to patterned surfaces when the radii of fibronectin nanodots were smaller than 100 nm. (Horzum et al., 2014; Pesen and Haviland, 2009) Therefore, we used a line dose of 1800 pAs/cm to fabricate protein nanodots with radii of 200 nm.

To study invadopodia, we used the MDA-MB-231 cell line because it is triple negative (estrogen receptor, progesterone receptor, epidermal growth factor receptor 2), of basal-like subtype, and is widely used as a highly invasive cell line model to specifically study invadopodia (Antelmi et al., 2013; Artym et al., 2006; Brenton et al., 2005; Brisson et al., 2013; Lizarraga et al., 2009; Macpherson et al., 2014; Magalhaes et al., 2011; Marchesin et al., 2015; Oxmann et al., 2008; Williams et al., 2014). MDA-MB-231 cells were starved and cultured in the presence of epidermal growth factor on control surfaces which were uniformly coated with fibronectin (FN), laminin (Lam), or K-casein (Kcas). FN and Lam are both extracellular matrix proteins and support cell adhesion while Kcas is a cell adhesion blocking protein. Cells neither adhered nor spread effectively on Kcas surfaces and thus did not support invadopodia formation (data not shown). Invadopodia were detected by co- immunofluorescence staining of actin and cortactin (Fig. 2a, b). Numbers of invadopodia per cell were detected with a semi-automatic approach (Fig. S1). Areas of cells cultured on FN control surfaces were 1.45 fold larger than those on Lam control surfaces ($1234 \pm 63\,\mu m^2$ vs. $851 \pm 56\,\mu m^2$, $p < 0.05$) (Figs. 2 c and S3, Table 1), suggesting that fibronectin promoted cell adhesion better than laminin. Numbers of cortactin-actin positive invadopodia per cell on FN control surfaces were similar to those on Lam control surfaces (4.80 ± 0.45 vs. 6.97 ± 1.16, $p < 0.09$ two-tailed Student's *t*-test, $p < 0.45$ two-tailed Mann-Whitney test) (Fig. 2d, Fig. S1). Invadopodia density, which was defined as the number of invadopodia divided by the area of the cell (Astro et al., 2011; Van Audenhove et al., 2016; van den Dries et al., 2012), was smaller on FN control surfaces than those on Lam control surfaces ($0.004 \pm 0.0004\,\mu m^{-2}$ vs. $0.008 \pm 0.001\,\mu m^{-2}$, $p < 0.05$) (Fig. 2e) suggesting that laminin may promote invadopodia formation better than fibronectin. Here, the difference in invadopodia density was in part due to differences in cell areas. The invadopodia number per cell on FN control surfaces was in agreement with previously reported values for gelatin coated surfaces (Beaty et al., 2013). Both FN and collagen I, of which gelatin is a hydrolysis product, are found in the connective tissue whereas Lam is

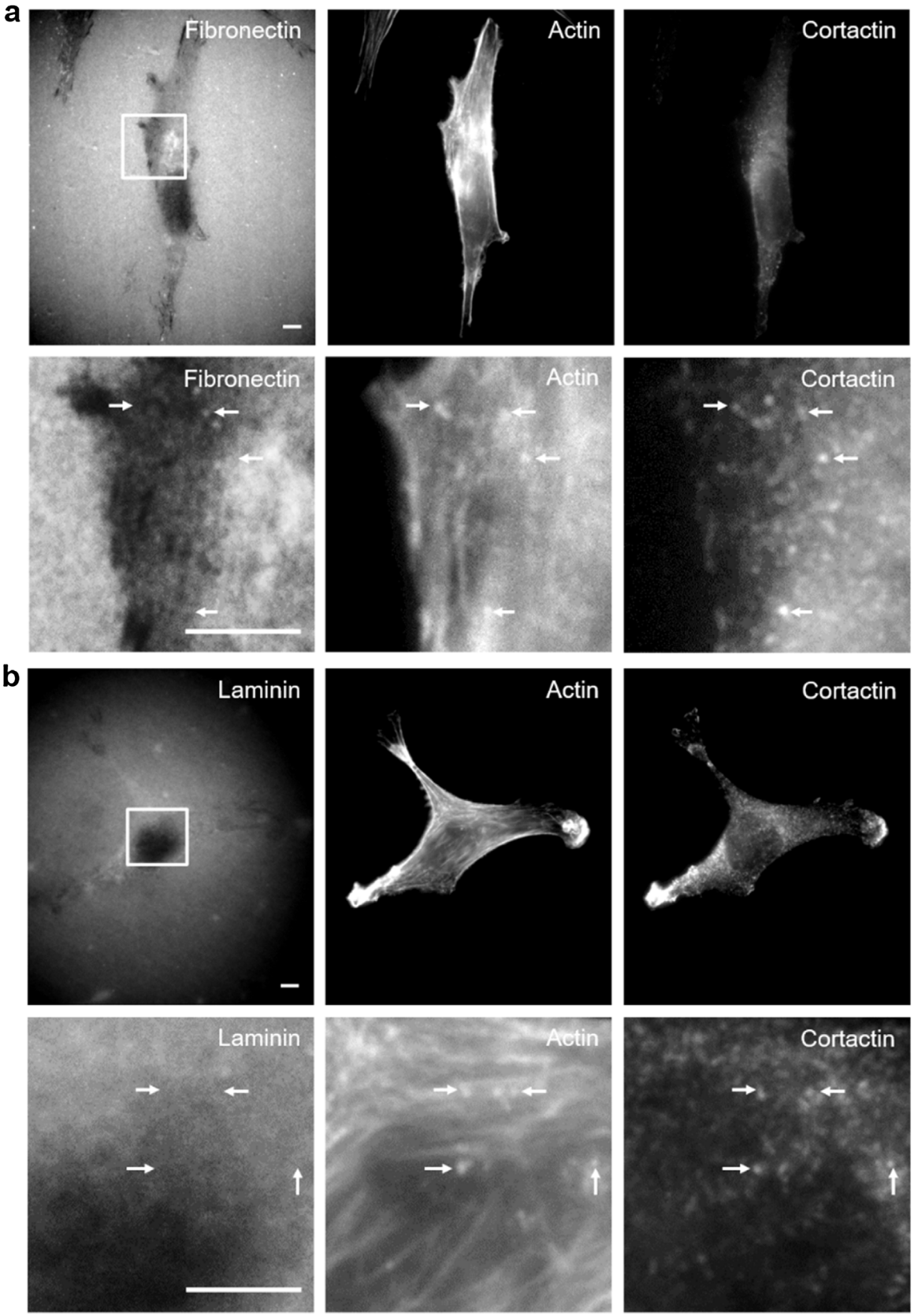

Fig. 2. Invadopodia formation on fibronectin and laminin control surfaces. Representative immunofluorescence images of breast cancer cells cultured on uniformly coated (a) fibronectin and (b) laminin surfaces are shown. Bottom panels show magnified images of the region of interest outlined in the top panels. Arrows point to cortactin and actin positive invadopodia. (c) Cell area (d) Invadopodia number per cell € Invadopodia density (f) Distribution of polarization values for cell area (g) Distribution of polarization values for invadopodia. (h) Polarization of invadopodia. Horizontal − vertical lines and asterisks show significant differences between groups and surfaces, respectively ($p < 0.05$). Scale bars 5 μm.

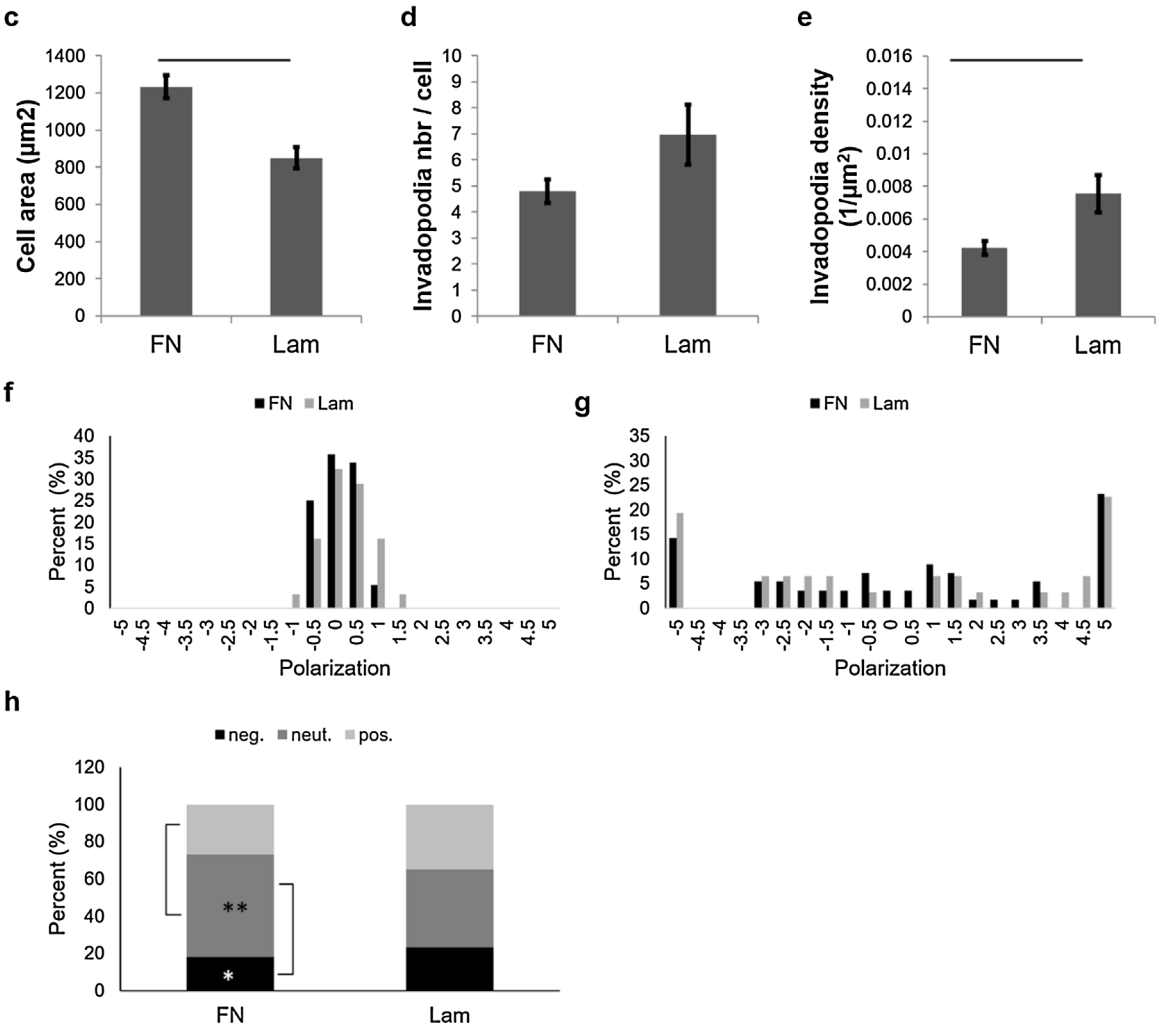

Fig. 2. (*continued*)

found in the basement membrane through which initial invasion by cancer cells takes place. Thus differences in the surface protein coatings may result in differences in invadopodia formation. (McCarthy et al., 1985)

Next, we investigated polarization values which were calculated based on a previously reported metric (Horzum et al., 2015; Polacheck et al., 2011). Polarization values show whether a parameter is evenly distributed or not based on spatial information. The spatial reference was chosen as the line passing through the geometric center of a cell. If the area of a cell was similar on both sides of this reference line, then the polarization of cell area was neutral. If the distribution of invadopodia was similar on both sides of this reference line, then the polarization of invadopodia was neutral. If more of the cell area was on one side of the spatial reference line, then the cell area was polarized. Polarization can be positive or negative. On isotropic surfaces, the spatial direction was random whereas on anisotropic surfaces, the direction where there were more protein nanodots was defined as the positive (up) direction. Mean polarization values for cell area and invadopodia were similar for FN and Lam control surfaces. (Table S2, Fig. S4). Polarization values were also grouped into three categories: negative, neutral and positive. For cell area, all cells were in the neutral group on all surfaces, (Figs. 2 f, 3 f, 4 f), in contrast to invadopodia ($p < 0.05$). For invadopodia, 18%, 55%, 27% and 23%, 42%, 35% of cells were classified as negative, neutral and positive, for FN and Lam surfaces, respectively, showing that there was an inherent polarization of invadopodia distribution unlike cell area (Fig. 2g, h). For FN surfaces, the percent of cells in the neutral group was higher than those in the negative and positive groups (55% vs. 18%, 55% vs. 27% $p < 0.05$). For Lam surfaces, the percentages of invadopodia polarization in the three groups were similar to each other (23%, 42%, and 35%). There were no differences between invadopodia polarization mean values and classification between FN and Lam surfaces (Tables S2 and 2). These results showed that invadopodia possessed an inherent polarization unlike cell area on FN and Lam control surfaces.

To study invadopodia on nanometer scale protein patterns, cells were cultured on KcasFN surfaces, which comprised FN nanodots on a K-casein background and on LamFN surfaces which comprised FN nanodots on a laminin background. Invadopodia were identified as actin and cortactin positive dots (Fig. 3a, b). Areas of cells on KcasFN surfaces were larger than those on LamFN surfaces ($1051 \pm 74\,\mu m^2$ vs. $649 \pm 113\,\mu m^2$, $p < 0.05$) (Fig. 3c), suggesting that laminin had a reducing effect on cell adhesion on LamFN surfaces, in agreement with results on Lam and FN control surfaces. Areas of cells on KcasFN and LamFN surfaces were smaller than those on FN and Lam control surfaces, respectively ($1233 \pm 63\,\mu m^2$ vs. $1051 \pm 74\,\mu m^2$; $851 \pm 56\,\mu m^2$ vs. $649 \pm 113\,\mu m^2$, $p < 0.05$) (Fig. S3, Table 1), indicating that presence of nanopatterns could reduce cell area. Numbers of cortactin-actin positive invadopodia per cell on KcasFN surfaces were smaller than those on LamFN surfaces (3.62 ± 0.43 vs. 7.23 ± 1.38, $p < 0.05$) (Fig. 3d), showing that laminin but not K-casein promoted invadopodia formation, as expected. Numbers of invadopodia were similar on Lam control and LamFN surfaces (Fig. S3, Table 1). On the other hand, numbers of invadopodia were lower on KcasFN surfaces than on FN control surfaces (3.61 ± 0.43 vs. 4.80 ± 0.45, $p < 0.05$)

Table 2
Polarization of invadopodia and the golgi complex.

Invadopodia	FN	Lam	KcasFN	LamFN	KcasFNg	LamFNg
% cells with negative polarization	18*	23	30	8	35*	31
% cells with neutral polarization	55**	42	34** ‡	62	48	56
% cells with positive polarization	27	35	36***	31	17***	13
Golgi complex	**FN**	**Lam**	**KcasFN**	**LamFN**	**KcasFNg**	**LamFNg**
% cells with negative polarization			14*	4	54* **	13**
% cells with neutral polarization			64 ‡	84	31***	71***
% cells with positive polarization			23	11	15	16

*, **, *** and ‡ show significant differences between different surfaces and between invadopodia and the golgi complex, respectively, $p < 0.05$. Total percent may not be 100 due to rounding.

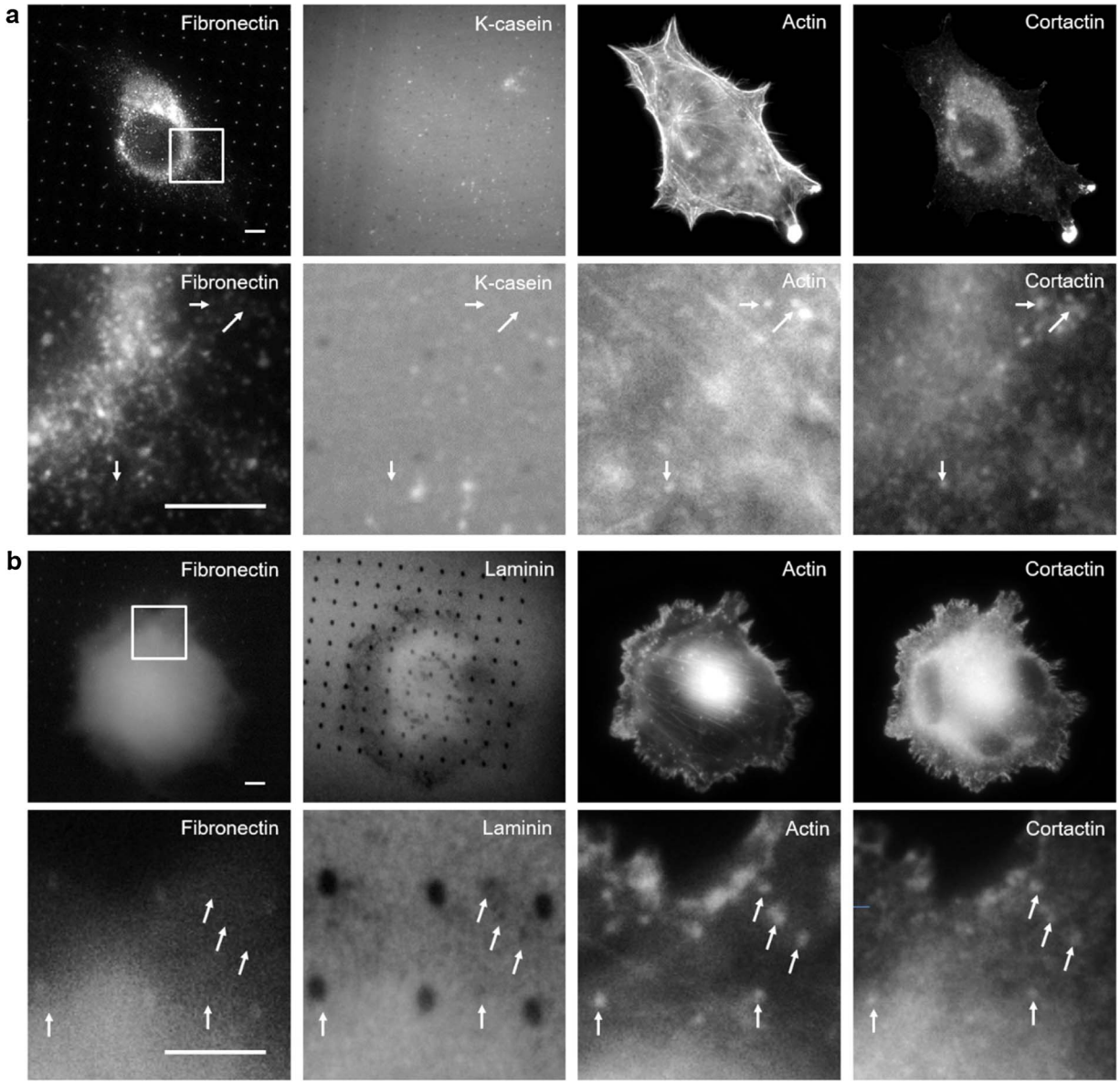

Fig. 3. Invadopodia formation on KcasFN and LamFN surfaces. Representative immunofluorescence images of breast cancer cells cultured on (a) KcasFN and (b) LamFN surfaces are shown. Bottom panels show magnified images of the region of interest outlined in the top panels. Arrows point to cortactin and actin positive invadopodia. (c) Cell area (d) Invadopodia number per cell (e) Invadopodia density (f) Distribution of polarization values for cell area (g) Distribution of polarization values for invadopodia. (h) Polarization of invadopodia. Horizontal − vertical lines and asterisks show significant differences between groups and surfaces, respectively ($p < 0.05$). Scale bars 5 μm.

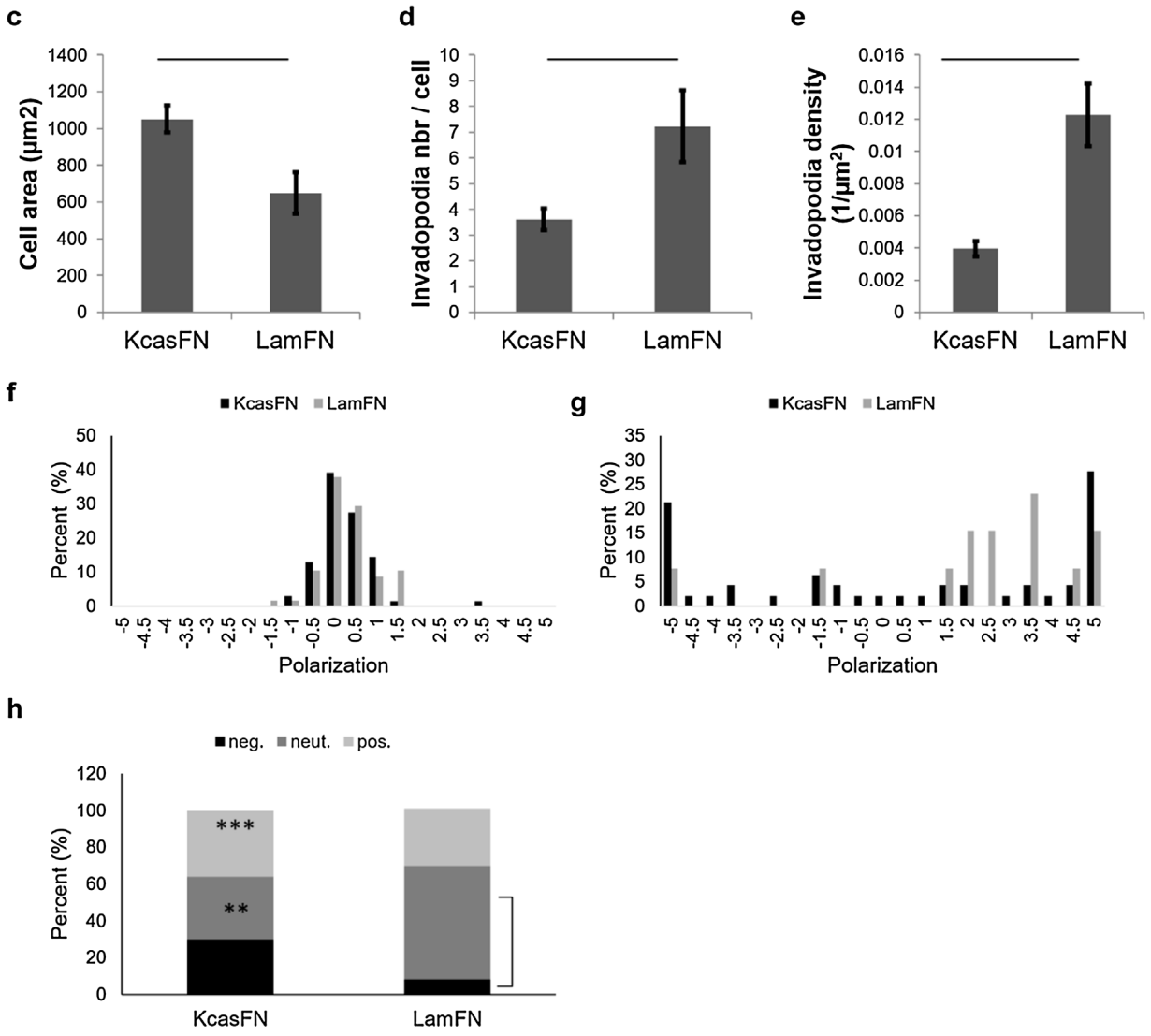

Fig. 3. (*continued*)

(Fig. S3, Table 1), indicating that presence of FN nanopatterns on a non-adhesive background could reduce invadopodia number per cell. In addition, invadopodia density was smaller on KcasFN surfaces than those on LamFN surfaces ($0.004 \pm 0.0005\,\mu m^{-2}$ vs. $0.012 \pm 0.002\,\mu m^{-2}$, $p < 0.05$) (Fig. 3e). Invadopodia density was higher on LamFN surfaces than on Lam control surfaces due to a combination of higher invadopodia number per cell and smaller cell area on LamFN surfaces (0.01 ± 0.002 vs. 0.008 ± 0.001, $p < 0.05$) (Fig. S3, Table 1). Invadopodia density on FN control and KcasFN surfaces were similar to each other. These results showed that both composition and organization of surface proteins regulated invadopodia formation.

Polarizations of cell area and invadopodia on KcasFN and LamFN surfaces were similar to those on control surfaces: Although cell area was not polarized, invadopodia distribution was (Fig. 3f, g). For LamFN surfaces, the percent of cells in the neutral group was higher than that in the negative group (62% vs. 8%, $p < 0.05$, Fig. 3 h). For KcasFN surfaces, the percentages of invadopodia polarization in the three groups were similar to each other (30%, 34%, and 36%). There were no differences between invadopodia polarization mean values and classification between KcasFN and LamFN surfaces (Table S2, Table 2). Interestingly, presence of nanopatterns, i.e. KcasFN surfaces, decreased percent of cells with neutral invadopodia polarization from 55% to 34% with respect to FN control surfaces ($p < 0.05$, Table 2, Figs. 2 h, 3 h). These results showed that adhesive nanopatterns on a non-adhesive background promoted polarization of invadopodia.

To determine whether anisotropic nanopatterns have an effect on invadopodia distribution, cells were cultured on gradient KcasFN (KcasFNg) and gradient LamFN (LamFNg) surfaces. Unlike KcasFN and LamFN surfaces where the spacing between FN dots was constant and 5 µm, on gradient surfaces the spacings changed from 1 µm up to 10 µm (Fig. 4a, b). Areas of cells on KcasFNg surfaces were larger than those on LamFNg surfaces ($896 \pm 42\,\mu m^2$ vs. $561 \pm 43\,\mu m^2$, $p < 0.05$) (Figs. 4 c, Fig. S3, Table 1), as was the case for isotropic KcasFN and LamFN surfaces. There were no differences in cell area between KcasFN and KcasFNg, LamFN and LamFNg surfaces (Fig. S3, Table 1). Interestingly, numbers of cortactin-actin positive invadopodia per cell on KcasFNg and LamFNg surfaces were similar to each other (Fig. 4d) unlike the case for FN vs. Lam control and KcasFN vs. LamFN surfaces (Figs. 2 d, 3 d). This might be due to presence of more fibronectin on the LamFNg surfaces than on LamFN surfaces. The distribution but not the mean number of invadopodia per cell was different between FN control and KcasFNg surfaces (4.80 ± 0.45 vs. 4.54 ± 0.71, $p < 0.75$ two-tailed Student's *t*-test, $p < 0.05$ two-tailed Mann-Whitney test) (Fig. S1, Fig. S3, Table 1). On the other hand, invadopodia density was smaller on KcasFNg surfaces than those on LamFNg surfaces ($0.005 \pm 0.0005\,\mu m^{-2}$ vs. $0.008 \pm 0.0008\,\mu m^{-2}$, $p < 0.05$) (Fig. 4e). Invadopodia density was lowest and similar for cells on FN

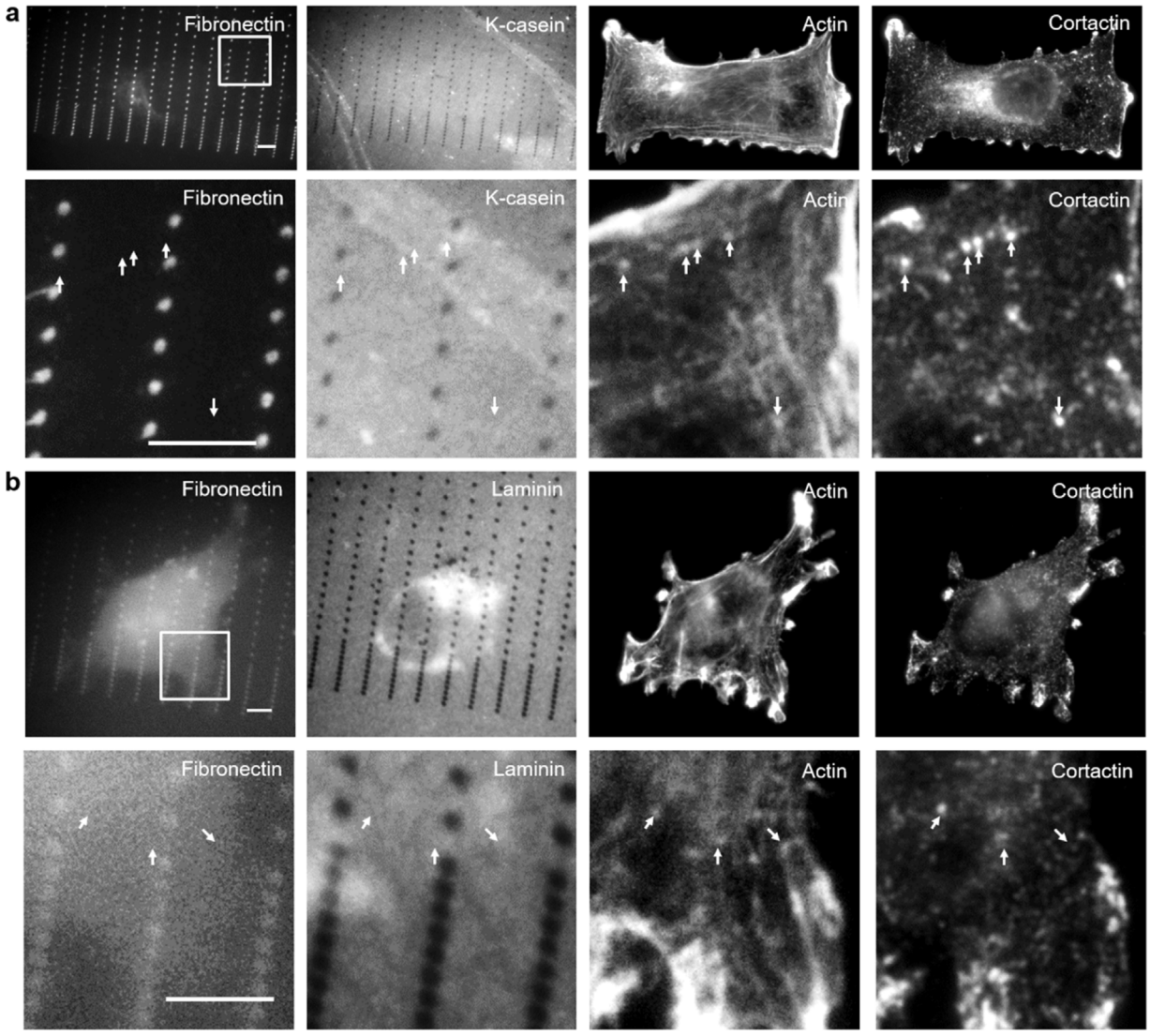

Fig. 4. Invadopodia formation on KcasFNg and LamFNg surfaces. Representative immunofluorescence images of breast cancer cells cultured on (a) KcasFNg and (b) LamFNg surfaces are shown. Bottom panels show magnified images of the region of interest outlined in the top panels. Arrows point to cortactin and actin positive invadopodia. (c) Cell area (d) Invadopodia number per cell (e) Invadopodia density (f) Distribution of polarization values for cell area (g) Distribution of polarization values for invadopodia. (h) Polarization of invadopodia. Horizontal − vertical lines and asterisks show significant differences between groups and surfaces, respectively ($p < 0.05$). Scale bars 5 μm.

control, KcasFN and KcasFNg surfaces, it was higher and similar for cells on Lam control and LamFNg surfaces and it was highest for cells on LamFN surfaces ($p < 0.05$) (Fig. S3, Table 1). Density of invadopodia was similar between same type of isotropic and gradient surfaces. These results suggested that the composition of nanopatterns was dominant over their organization for regulating invadopodia formation.

There was a small but significant difference in cell area polarization between KcasFNg and LamFNg surfaces (-0.11 ± 0.06 vs. 0.08 ± 0.07, $p < 0.05$), i.e. more of the cell area was on the K-casein background of the KcasFNg surfaces and on the fibronectin rich part of the LamFNg surfaces (Table S2, Fig. S4). However, all cells were in the neutral group on all surfaces. Invadopodia on the other hand showed significant polarization (Fig. 4g): For KcasFNg surfaces, the percent of cells in the neutral group was higher than that in the positive group (48% vs. 17%, $p < 0.05$, Table 2, Fig. 4h). For LamFNg surfaces, the percent of cells in the neutral group was higher than those in the positive group (56% vs. 13%, $p < 0.05$, Table 2, Fig. 4h). There were no differences between invadopodia polarization mean values and classification between KcasFNg and LamFNg surfaces (Tables S2, 2). However, mean polarization of invadopodia on KcasFNg surfaces was smaller than that on FN surfaces (-1.01 ± 0.48 vs. 0.33 ± 0.46, $p < 0.05$, Table S2, Fig. S4). Thus KcasFNg surfaces promoted negative polarization of invadopodia. Mean polarization of invadopodia on LamFNg surfaces was also smaller than that on LamFN surfaces (-1.24 ± 0.80 vs. 2.04 ± 0.76, $p < 0.05$, Table S2, Fig. S4). Thus LamFNg surfaces also promoted negative polarization of invadopodia. What is more, presence of a gradient, i.e. KcasFNg surfaces, decreased percent of cells with positive invadopodia polarization from 36% to 17% with respect to KcasFN surfaces ($p < 0.05$, Table 2, Figs. 3 h, 4 h). Furthermore, presence of both nanopatterns and a gradient, i.e. KcasFNg surfaces, increased percent of cells with negative invadopodia polarization from 18% to 35% with respect to FN control surfaces ($p < 0.05$, Table 2, Figs. 2 h, 4 h). These results showed that gradient adhesive nanopatterns on a non-adhesive (K-casein) or Lam background promoted negative polarization of invadopodia, which in turn, suggested a lack of a local adhesion requirement or preference for laminin.

As invadopodia appear in close proximity to the golgi complex the position of which can be modulated by micrometer scale surface patterns, we examined polarization of the golgi complex on isotropic and gradient KcasFN and LamFN surfaces. Cells were cultured on nanopatterned surfaces under the same conditions for the invadopodia assays. The golgi complex was immunostained, imaged with a

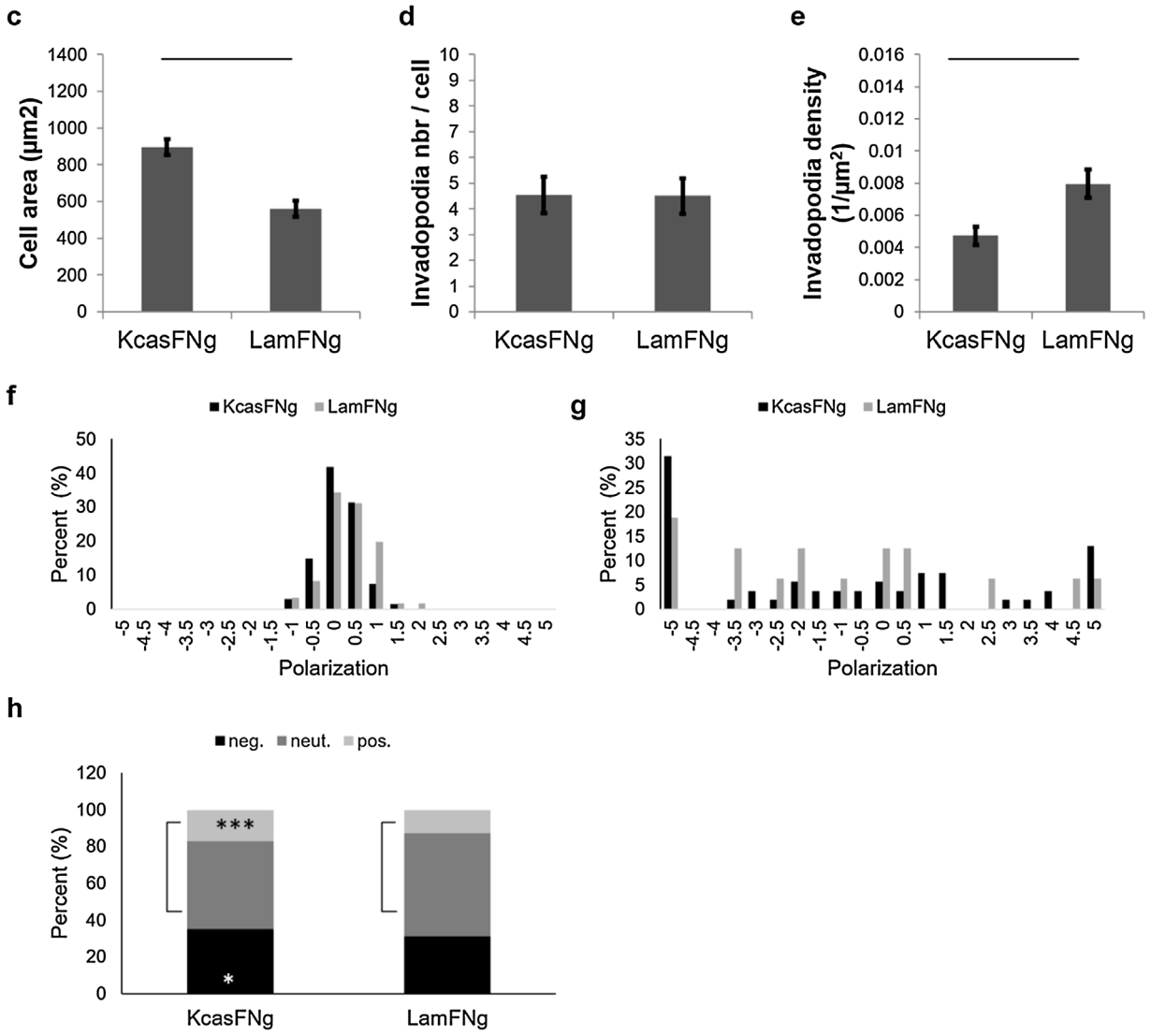

Fig. 4. (*continued*)

fluorescence microscope and polarization was calculated as it was performed using the mean fluorescence intensity of the golgi complex. The mean polarization values for the golgi complex were similar to each other except that mean polarization on KcasFNg surfaces was smaller than that on LamFN surfaces, (-1.66 ± 0.94 vs. 0.11 ± 0.34, $p < 0.05$, Table S2, Fig. S4). The polarization of cell area and golgi were similar to each other except that mean polarization of golgi was smaller than that of cell area on KcasFNg surfaces (-1.66 ± 0.94 vs. -0.11 ± 0.06, $p < 0.05$, Table S2, Fig. S4). Thus presence of a gradient of adhesive nanopatterns on a non-adhesive background induced polarization of the golgi complex more effectively than that of cell area. On KcasFNg surfaces both the golgi complex and invadopodia preferred the non-adhesive background part of the surface, in agreement with a spatial link between golgi and invadopodia (mean polarization values -1.66 ± 0.94 and -1.01 ± 0.48, respectively, $p < 0.94$, Table S2, Fig. S4). The polarization of invadopodia and golgi were similar to each other except that mean polarization of golgi was smaller than that of invadopodia on LamFN surfaces (0.11 ± 0.34 vs. 2.04 ± 0.76, $p < 0.05$, Table S2, Fig. S4). Therefore, presence of laminin as the background of FN nanopatterns promoted the inherent polarization for invadopodia better than that for the golgi complex. The golgi complex was inherently polarized on isotropic nanopatterned surfaces unlike cell area but similar to invadopodia. For KcasFN surfaces the percent of cells in the neutral group was higher than those in the positive and negative groups (64% vs. 14%, 64% vs. 23% $p < 0.05$, Fig. 5 g, Table 2). For LamFN surfaces, the percent of cells in the neutral group was higher than those in the positive and negative groups (84% vs. 4%, 84% vs. 11%, $p < 0.05$, Fig. 5g, Table 2). For LamFNg surfaces the percent of cells in the neutral group was higher than those in the positive and negative groups (71% vs. 13%, 71% vs. 16%, $p < 0.05$, Fig. 5h, Table 2). For KcasFNg surfaces, the distribution of golgi polarization in the three groups were similar. Interestingly, presence of a gradient of nanopatterns, i.e. KcasFNg surfaces, increased percent of cells with negative golgi polarization from 14% to 54% with respect to KcasFN surfaces ($p < 0.05$, Table 2, Fig. 5g, h). What is more, percent of cells with negative golgi polarization was higher on KcasFNg surfaces than that on LamFNg surfaces (54% vs. 13%, $p < 0.05$, Table 2, Fig. 5h). In addition, percent of cells with neutral golgi polarization was smaller on KcasFNg surfaces than that on LamFNg surfaces (31% vs. 71%, $p < 0.05$, Table 2, Fig. 5h). These results showed that a gradient of adhesive nanopatterns on a non-adhesive background promoted polarization of the golgi complex, as was the case for invadopodia. The classification of polarization of invadopodia and the golgi complex were similar on the same type of surfaces except on KcasFN surfaces where more cells were in the neutral group for golgi polarization than that for invadopodia polarization (64% vs 34%, $p < 0.05$, Table 2, Figs. 3 h, 5 g). Thus presence adhesive nanopatterns on a non-adhesive background was more effective in promoting polarization of invadopodia than that

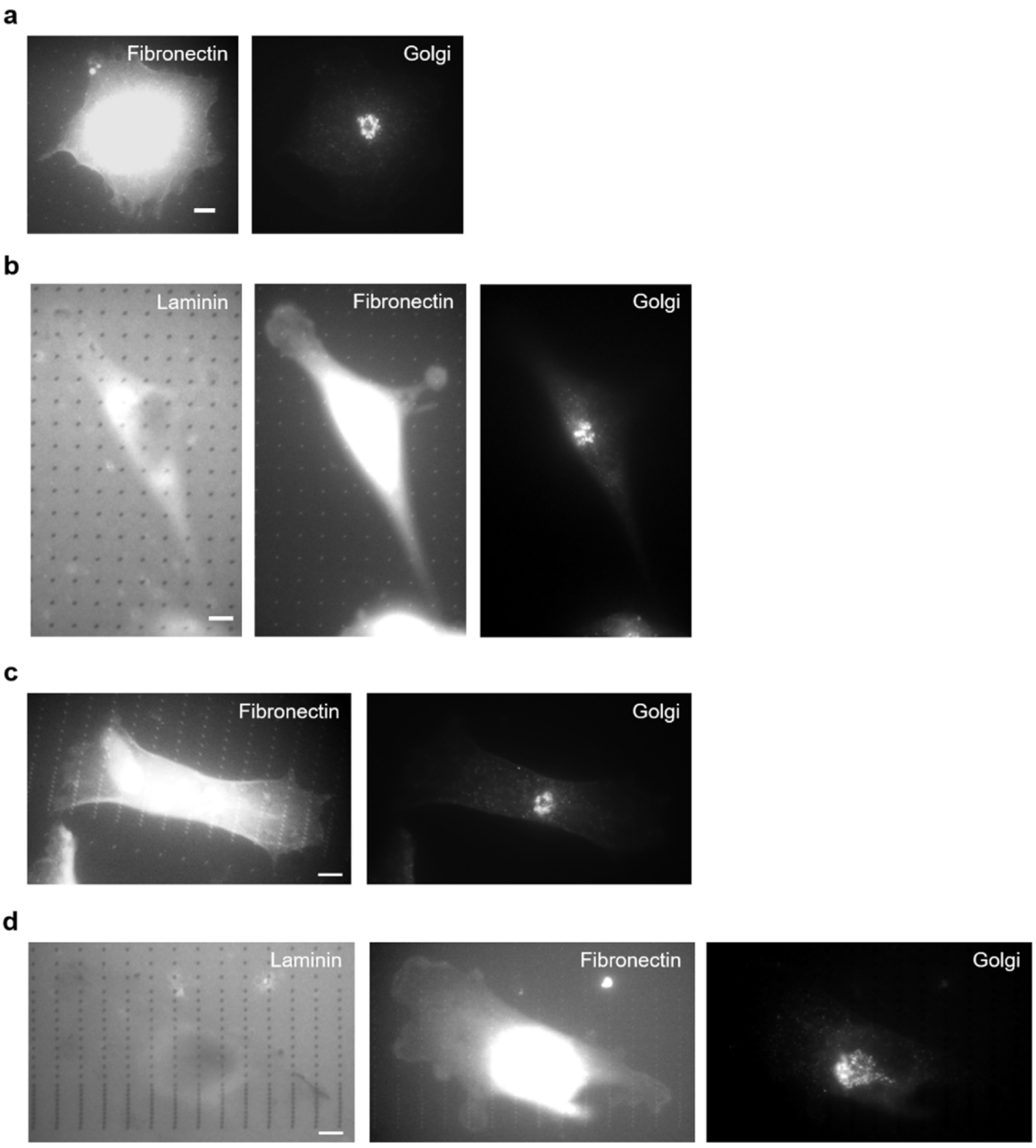

Fig. 5. The golgi complex on nanopatterned surfaces. Representative immunofluorescence images of breast cancer cells cultured on (a) KcasFN, (b) KcasFNg, (c) LamFN and (d) LamFNg surfaces are shown. Distribution of polarization values for the golgi complex on (e) isotropic and (f) gradient surfaces. Polarization of the golgi complex on isotropic (g) and gradient surfaces (h). Vertical lines and asterisks show significant differences between groups and surfaces, respectively ($p < 0.05$). Scale bars 5 μm.

of the golgi complex. These results showed that nanopatterned surfaces can polarize both invadopodia and the golgi complex, in agreement with a spatial link between golgi and invadopodia.

Invadopodia are related to podosomes which also have proteolytic activity. The most agreed upon distinction between podosomes and invadopodia is that podosomes form in normal cells whereas invadopodia form in cancer cells. Vinculin, which is a focal adhesion protein, is also a marker for podosomes although some studies accept vinculin as a marker for invadopodia as well. Previous studies have shown that focal adhesions, of which vinculin is an accepted marker, prefer fibronectin rich areas on protein nanopatterns (Horzum et al., 2014; Horzum et al., 2015). Our results showed that areas of cells on fibronectin control and KcasFN surfaces were similar to each other, i.e. these surfaces supported global cell adhesion. In addition, immunofluorescence labeling of vinculin and cortactin and actin showed no colocalization (Fig. S5). What is more, fibronectin promoted cell adhesion better than laminin since presence of laminin reduced areas of cells; laminin appeared to be a less-adhesive protein. Percent of cells with negative invadopodia polarization was higher on KcasFNg than on FN control surfaces (35% vs. 18%, $p < 0.05$, Table 2, Figs. 2 h, 4 h). Furthermore, the percent of cells with positive invadopodia polarization was lower on KcasFNg than on KcasFN surfaces (17% vs. 36%, $p < 0.05$, Table 2, Figs. 3 h, 4 h). Together these findings suggested that local adhesion was not necessarily a prerequisite for invadopodia formation and lack of a requirement for local adhesion may be used as another distinction between invadopodia and podosomes.

To the best of our knowledge, we provided the first study of invadopodia on nanometer scale protein patterns. Custom nanopatterned surfaces, in particular gradient surfaces, used here provided original insights into how both the composition and the organization of surface protein nanopatterns could regulate formation and distribution of invadopodia which are important in cancer cell biology. These surfaces

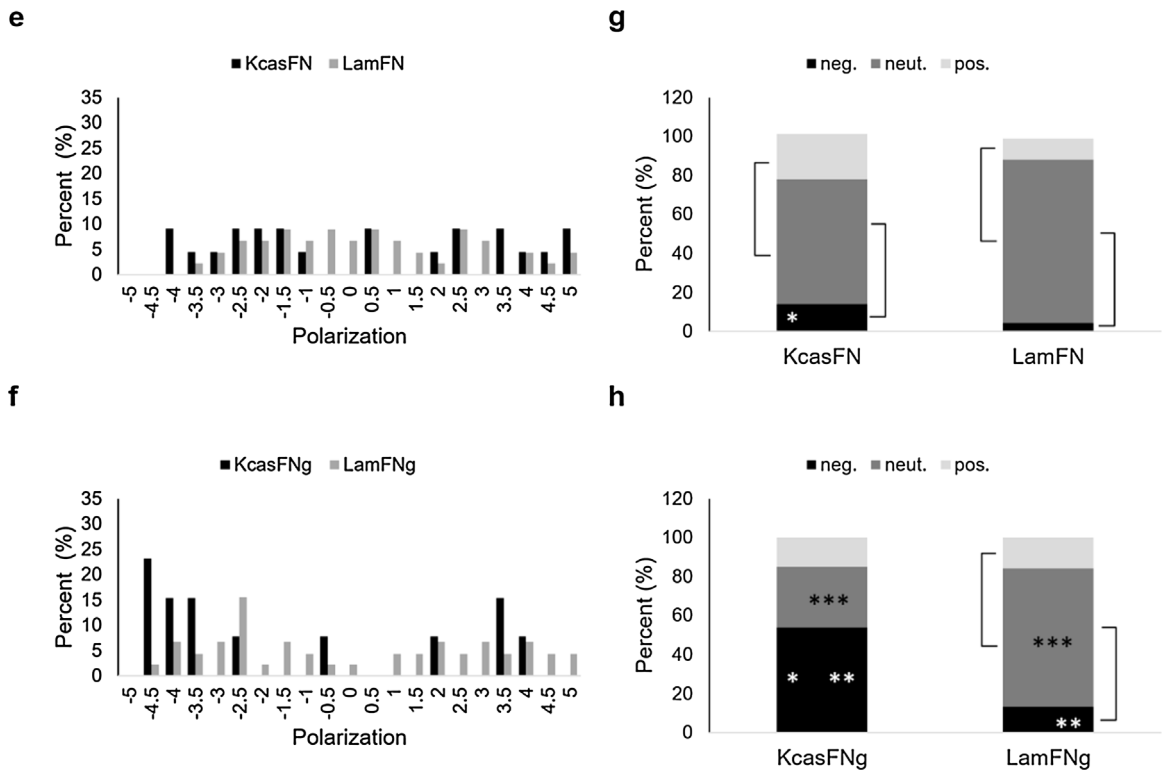

Fig. 5. (*continued*)

offer a new platform to investigate how extracellular surface signals modulate intracellular organization, and thus are expected to help to develop innovative paradigms for cellular structures and their functions.

Author contributions

D.P-O. conceived and supervised the study and designed the experiments; G.B. performed experiments and D.P-O. contributed to parts of it; G.B., A.C. and D.P-O. analyzed data; D.P-O. wrote and revised the manuscript and G.B. contributed to parts of it.

Funding sources

This work was supported by The Scientific and Technological Research Council of Turkey (TUBITAK) Grant 111T547. Samples were fabricated in the Applied Quantum Research Center at Izmir Institute of Technology, supported by State Planning Organization (DPT) Grant 2009K120860.

Acknowledgment

We thank Assoc. Prof. Ozden Yalcin-Ozuysal and Assoc. Prof. Engin Ozcivici for helpful discussions and Dr. Ebru Koc from Izmir Institute of Technology Academic Writing Center for assisting with English language editing.

Appendix A. Supplementary data

Supplementary data associated with this article can be found, in the online version, at http://dx.doi.org/10.1016/j.ejcb.2017.08.001.

References

Agheli, H., Malmstrom, J., Larsson, E.M., Textor, M., Sutherland, D.S., 2006. Large area protein nanopatterning for biological applications. Nano Lett. 6, 1165–1171.

Anderegg, F., Geblinger, D., Horvath, P., Charnley, M., Textor, M., Addadi, L., Geiger, B., 2011. Substrate adhesion regulates sealing zone architecture and dynamics in cultured osteoclasts. PLoS One 6.

Antelmi, E., Cardone, R.A., Greco, M.R., Rubino, R., Di Sole, F., Martino, N.A., Casavola, V., Carcangiu, M., Moro, L., Reshkin, S.J., 2013. Beta 1 integrin binding phosphorylates ezrin at T567 to activate a lipid raft signalsome driving invadopodia activity and invasion. PLoS One 8.

Artym, V.V., Zhang, Y., Seillier-Moiseiwitsch, F.O., Yamada, K.M., Mueller, S.C., 2006. Dynamic interactions of cortactin and membrane type 1 matrix metalloproteinase at invadopodia: defining the stages of invadopodia formation and function. Cancer Res. 66, 3034–3043.

Astro, V., Asperti, C., Cangi, G., Doglioni, C., de Curtis, I., 2011. Liprin-alpha 1 regulates breast cancer cell invasion by affecting cell motility, invadopodia and extracellular matrix degradation. Oncogene 30, 1841–1849.

Baldassarre, M., Pompeo, A., Beznoussenko, G., Castaldi, C., Cortellino, S., McNiven, M.A., Luini, A., Buccione, R., 2003. Dynamin participates in focal extracellular matrix degradation by invasive cells. Mol. Biol. Cell 14, 1074–1084.

Bat, E., Lee, J., Lau, U.Y., Maynard, H.D., 2015. Trehalose glycopolymer resists allow direct writing of protein patterns by electron-beam lithography. Nat. Commun. 6.

Bati, G., Okvur, D.P., 2014. Invadopodia: proteolytic feet of cancer cells. Turk. J. Biol. 38, 740–747.

Beaty, B.T., Sharma, V.P., Bravo-Cordero, J.J., Simpson, M.A., Eddy, R.J., Koleske, A.J., Condeelis, J., 2013. beta 1 integrin regulates Arg to promote invadopodial maturation and matrix degradation. Mol. Biol. Cell 24, 1661–1675.

Bowden, E.T., Onikoyi, E., Slack, R., Myoui, A., Yoneda, T., Yamada, K.M., Mueller, S.C., 2006. Co-localization of cortactin and phosphotyrosine identifies active invadopodia in human breast cancer cells. Exp. Cell Res. 312, 1240–1253.

Brenton, J.D., Carey, L.A., Ahmed, A.A., Caldas, C., 2005. Molecular classification and molecular forecasting of breast cancer: ready for clinical application? J. Clin. Oncol. 23, 7350–7360.

Brisson, L., Driffort, V., Benoist, L., Poet, M., Counillon, L., Antelmi, E., Rubino, R., Besson, P., Labbal, F., Chevalier, S., Reshkin, S.J., Gore, J., Roger, S., 2013. Na(V)1.5 Na+ channels allosterically regulate the NHE-1 exchanger and promote the activity of breast cancer cell invadopodia. J. Cell Sci. 126, 4835–4842.

Buccione, R., Caldieri, G., Ayala, I., 2009. Invadopodia: specialized tumor cell structures for the focal degradation of the extracellular matrix. Cancer Metastasis Rev. 28, 137–149.

Caldieri, G., Buccione, R., 2010. Aiming for invadopodia: organizing polarized delivery at sites of invasion. Trends Cell Biol. 20, 64–70.

Cavalcanti-Adam, E.A., Volberg, T., Micoulet, A., Kessler, H., Geiger, B., Spatz, J.P., 2007. Cell spreading and focal adhesion dynamics are regulated by spacing of integrin ligands. Biophys. J . 92, 2964–2974.

DesMarais, V., Yamaguchi, H., Oser, M., Soon, L., Mouneimne, G., Sarmiento, C., Eddy, R., Condeelis, J., 2009. N-WASP and cortactin are involved in invadopodium-dependent chemotaxis to EGF In Breast tumor cells. Cell Motil. Cytoskeleton 66, 303–316.

Destaing, O., Block, M.R., Planus, E., Albiges-Rizo, C., 2011. Invadosome regulation by

adhesion signaling. Curr. Opin. Cell Biol. 23, 597–606.
Gimona, M., Buccione, R., Courtneidge, S.A., Linder, S., 2008. Assembly and biological role of podosomes and invadopodia. Curr. Opin. Cell Biol. 20, 235–241.
Horzum, U., Ozdil, B., Pesen-Okvur, D., 2014. Micrometer scale spacings between fibronectin nanodots regulate cell morphology and focal adhesions. Mater. Res. Express 1, 025402.
Horzum, U., Ozdil, B., Pesen-Okvur, D., 2015. Differentiation of normal and cancer cell adhesion on custom designed protein nanopatterns. Nano Lett. 15, 5393–5403.
Labernadie, A., Thibault, C., Vieu, C., Maridonneau-Parini, I., Charriere, G.M., 2010. Dynamics of podosome stiffness revealed by atomic force microscopy. Proc. Natl. Acad. Sci. U. S. A. 107, 21016–21021.
Linder, S., Aepfelbacher, M., 2003. Podosomes: adhesion hot-spots of invasive cells. Trends Cell Biol. 13, 376–385.
Linder, S., Wiesner, C., Himmel, M., 2011. Degrading devices: invadosomes in proteolytic cell invasion. In: In: Schekman, R., Goldstein, L., Lehmann, R. (Eds.), Annual Review of Cell and Developmental Biology, vol. 27. pp. 185–211.
Linder, S., 2009. Invadosomes at a glance. J. Cell Sci. 122, 3009–3013.
Lizarraga, F., Poincloux, R., Romao, M., Montagnac, G., Le Dez, G., Bonne, I., Rigaill, G., Raposo, G., Chavrier, P., 2009. Diaphanous-related formins are required for invadopodia formation and invasion of breast tumor cells. Cancer Res. 69, 2792–2800.
MacGrath, S.M., Koleske, A.J., 2012. Cortactin in cell migration and cancer at a glance. J. Cell Sci. 125, 1621–1626.
Macpherson, I.R., Rainero, E., Mitchell, L.E., van den Berghe, P.V.E., Speirs, C., Dozynkiewicz, M.A., Chaudhary, S., Kalna, G., Edwards, J., Timpson, P., Norman, J.C., 2014. CLIC3 controls recycling of late endosomal MT1-MMP and dictates invasion and metastasis in breast cancer. J. Cell Sci. 127, 3893–3901.
Mader, C.C., Oser, M., Magalhaes, M.A.O., Bravo-Cordero, J.J., Condeelis, J., Koleske, A.J., Gil-Henn, H., 2011. An EGFR-Src-Arg-Cortactin pathway mediates functional maturation of invadopodia and Breast cancer cell invasion. Cancer Res. 71, 1730–1741.
Magalhaes, M.A.O., Larson, D.R., Mader, C.C., Bravo-Cordero, J.J., Gil-Henn, H., Oser, M., Chen, X.M., Koleske, A.J., Condeelis, J., 2011. Cortactin phosphorylation regulates cell invasion through a pH-dependent pathway. J. Cell Biol. 195, 903–920.
Marchesin, V., Montagnac, G., Chavrier, P., 2015. ARF6 promotes the formation of rac1 and WAVE-dependent ventral F-actin rosettes in breast cancer cells in response to epidermal growth factor. PLoS One 10.
McCarthy, J.B., Basara, M.L., Palm, S.L., Sas, D.F., Furcht, L.T., 1985. The role of cell-adhesion proteins − laminin and fibronectin − in the movement of malignant and metastatic cells. Cancer Metastasis Rev. 4, 125–152.
Oser, M., Yamaguchi, H., Mader, C.C., Bravo-Cordero, J.J., Arias, M., Chen, X.M., DesMarais, V., van Rheenen, J., Koleske, A.J., Condeelis, J., 2009. Cortactin regulates cofilin and N-WASp activities to control the stages of invadopodium assembly and maturation. J. Cell Biol. 186, 571–587.
Oser, M., Mader, C.C., Gil-Henn, H., Magalhaes, M., Bravo-Cordero, J.J., Koleske, A.J., Condeelis, J., 2010. Specific tyrosine phosphorylation sites on cortactin regulate Nck1-dependent actin polymerization in invadopodia. J. Cell Sci. 123, 3662–3673.
Oxmann, D., Held-Feindt, J., Stark, A.M., Hattermann, K., Yoneda, T., Mentlein, R., 2008. Endoglin expression in metastatic breast cancer cells enhances their invasive phenotype. Oncogene 27, 3567–3575.
Pesen, D., Haviland, D.B., 2009. Modulation of cell adhesion complexes by surface protein patterns. ACS Appl. Mater. Interfaces 1, 543–548.
Pesen, D., Erlandsson, A., Ulfendahl, M., Haviland, D.B., 2007. Image reversal for direct electron beam patterning of protein coated surfaces. Lab Chip 7, 1603–1606.
Polacheck, W.J., Charest, J.L., Kamm, R.D., 2011. Interstitial flow influences direction of tumor cell migration through competing mechanisms. Proc. Natl. Acad. Sci. U. S. A. 108, 11115–11120.
Stylli, S.S., Kaye, A.H., Lock, P., 2008. Invadopodia: at the cutting edge of tumour invasion. J. Clin. Neurosci. 15, 725–737.
Thery, M., Racine, V., Piel, M., Pepin, A., Dimitrov, A., Chen, Y., Sibarita, J.B., Bornens, M., 2006. Anisotropy of cell adhesive microenvironment governs cell internal organization and orientation of polarity. Proc. Natl. Acad. Sci. U. S. A. 103, 19771–19776.
Van Audenhove, I., Denert, M., Boucherie, C., Pieters, L., Cornelissen, M., Gettemans, J., 2016. Fascin rigidity and L-plastin flexibility cooperate in cancer cell invadopodia and filopodia. J. Biol. Chem. 291, 9148–9160.
Williams, K.C., McNeilly, R.E., Coppolino, M.G., 2014. SNAP23, Syntaxin4, and vesicle-associated membrane protein 7 (VAMP7) mediate trafficking of membrane type 1-matrix metalloproteinase (MT1-MMP) during invadopodium formation and tumor cell invasion. Mol. Biol. Cell 25, 2061–2070.
Yamaguchi, H., Lorenz, M., Kempiak, S., Sarmiento, C., Coniglio, S., Symons, M., Segall, J., Eddy, R., Miki, H., Takenawa, T., Condeelis, J., 2005. Molecular mechanisms of invadopodium formation: the role of the N-WASP-Arp2/3 complex pathway and cofilin. J. Cell Biol. 168, 441–452.
van den Dries, K., van Helden, S.F.G., te Riet, J., Diez-Ahedo, R., Manzo, C., Oud, M.M., van Leeuwen, F.N., Brock, R., Garcia-Parajo, M.F., Cambi, A., Figdor, C.G., 2012. Geometry sensing by dendritic cells dictates spatial organization and PGE(2)-induced dissolution of podosomes. Cell. Mol. Life Sci. 69, 1889–1901.